Cellular and Molecular Bioengineering, Vol. 2, No. 1, March 2009 *(© 2009)* pp. 66–74
DOI: 10.1007/s12195-009-0047-9

Nanomechanical Characterization of the Triple β-Helix Domain in the Cell Puncture Needle of Bacteriophage T4 Virus

SINAN KETEN,[1] J. FERNANDO RODRIGUEZ ALVARADO,[2] SINAN MÜFTÜ,[3] and MARKUS J. BUEHLER[1]

[1]Laboratory for Atomistic and Molecular Mechanics, Department of Civil and Environmental Engineering, Massachusetts Institute of Technology, 77 Massachusetts Ave. Room 1-235A&B, Cambridge, MA, USA; [2]Department of Mechanical Engineering, Massachusetts Institute of Technology, 77 Massachusetts Ave., Cambridge, MA, USA; and [3]Department of Mechanical and Industrial Engineering, Northeastern University, 334 Snell Engineering Center, 360 Huntington Avenue, Boston, MA, USA

(Received 15 December 2008; accepted 2 February 2009; published online 18 February 2009)

Abstract—Beta-solenoids are a class of protein nanotube structures that are observed in virulence factors, prion proteins and amyloid fibrils. Here we investigate the compressive strength of the triple-beta-helix solenoid structure found in the cell puncture needle of the bacteriophage T4 virus. We characterize the compressive mechanical strength of this protein nanotube using full-atomistic molecular dynamics simulations in explicit solvent over a wide range of deformation speeds. We observe that the dynamical behavior, stiffness and failure strength of the structure are strongly dependent on the deformation rate. We illustrate that H-bond rupture initiation is the atomistic mechanism that leads to instability and buckling of the protein nanotube at the peak force. We show that the behavior of the protein under small compressive deformation can be approximated by a rate-dependent linear elastic modulus, which can be used in context of a continuum Euler buckling formula for the triple-helix geometry to predict the failure load. Our work provides a link between the structure and biofunctional properties of this beta-solenoid topology, and illustrates a rigorous framework for bridging the gap between experimental and simulation time-scales for future compression studies on proteins. Our study is relevant to self-assembling peptide nanotube materials, and may provide insight into the influence of mechanical properties on the pathological pathways of virulence factors, prions and amyloids found in neurodegenerative diseases.

Keywords—Protein, Nanotube, Triple beta-helix, Beta-solenoids, Buckling, Failure, Mechanics, Rate-dependence, Molecular dynamics, Hydrogen bond, Cell-puncture device, Amyloids.

INTRODUCTION

Beta-solenoid topologies are a recently discovered class of protein structures that typically exhibit highly ordered tubular or helical folds, consisting of beta-strands separated by loop regions.[3,17,38,39] This largely unexplored group of biomolecules has recently gained notable interest by scientists and engineers due to several reasons. First, they have been associated with a variety of biological functions that show promise for biotechnology applications, for instance as antifreeze proteins[12] or enzymes.[39] Second, they have been proposed as model structures for amyloids and prion proteins[8,11,23,34] that are associated with a vast variety of diseases ranging from Alzheimer's to mad cow disease.[7] Third, they form a universal structural protein motif in viral fibers and virulence factors, perhaps most notably in the cell puncture device needle of the bacteriophage T4 virus.[17,18,27]

Single molecule biophysics techniques[13] are commonly used to experimentally characterize mechanical and thermodynamical properties of proteins by subjecting them to tensile external forces. Atomic force microscopy (AFM) and optical tweezers (OT) studies coupled with steered molecular dynamics (SMD) simulations have been very fruitful in the past for explaining mechanical resistance of titin and fibronectin domains found in the extracellular matrix, and have also been applied to understand molecular mechanisms of failure in collageneous tissue.[4,5,16,26,33,37] More recently, computational and experimental techniques have focused on mechanical properties of amyloid proteins and fibrils in an effort to understand feasibility of using these materials for technological applications and for elucidating pathological pathways of related diseases.[1,19,24,28,35] Apart from a preliminary study we carried out on a similar protein structure,[20] there exist virtually no direct experimental or computational studies on the mechanical properties of beta-helix or beta-solenoid type structures, despite the fact that they serve obvious and important mechanical functions as part of viral infection mechanisms and have been

Address correspondence to Markus J. Buehler, Laboratory for Atomistic and Molecular Mechanics, Department of Civil and Environmental Engineering, Massachusetts Institute of Technology, 77 Massachusetts Ave. Room 1-235A&B, Cambridge, MA, USA. Electronic mail: mbuehler@mit.edu

proposed as model structures for amyloids. Despite recent advancements in our understanding of rate- and topology-dependent strength of protein materials,[21,22] to the best of our knowledge, there also exist no molecular dynamics studies on the rate-dependent compressive behavior of protein structures under external load.

Here we carry out a systematic nanomechanical characterization of the triple-beta-helix structure of the cell puncture device needle of the bacteriophage T4 virus, using massively parallelized molecular dynamics (MD) simulations. We study the behavior of this structure under compressive loading, as in the case of physiological conditions, and investigate the rate-dependent strength and stiffness of the molecule over four orders of magnitude in deformation rates. We show that the stiffness and failure strength of the molecule depend strongly on the rate of deformation and we present analytical functions to predict rate-dependence. We observe H-bond rupture initiation as the atomistic mechanism of instability corresponding to the peak load in the force extension curve. We illustrate that the behavior of the protein in small compressive deformation range can be approximated by a rate-dependent linear elastic modulus, which can be used in context of a continuum Euler buckling formula for the triple-helix geometry to predict critical load at failure over a small range of time scales. The atomistically-informed continuum mechanics predictions agree well with results from simulations. Our work provides a structure-property-function relationship for this beta-topology in line with the materials science paradigm. The approaches presented here illustrate a rigorous framework for bridging the gap between experimental and simulation time-scales for future single molecule biophysics experiments aimed at probing compressive strength of proteins. Our results are of significance for self-assembling peptide applications of peptide nanotubes, where mechanical properties influence formation and failure of bundles. Furthermore, mechanical characterization of beta-structures such as beta-solenoids and amyloids may provide crucial insight into viral infection mechanisms and the influence of mechanical properties on the pathological pathways of neurodegenerative diseases.

METHODS

Atomistic Model Setup and Equilibration

The coordinates for the molecular model (monomer) are obtained from the Protein Data Bank,[2] PDB file ID 1k28. The trimer is built by rotating the monomer structure around the helical axis and creating duplicates in a single coordinate file. The molecular assembly is truncated at the end of the gp5C domain and protein structure and coordinate files of this triple-beta-helix domain is created using psfgen tool in NAMD using CHARMM topology and parameter files.[25] The assembly is then minimized for 10,000 steps and equilibrated in a TIP3 water box of dimensions 6 nm × 6 nm × 12 nm for 1.2 ns, with periodic boundary conditions. Simulations are carried out in an *NPT* ensemble using the Langevin piston Nose–Hoover method implemented in the NAMD software.[30] A Langevin piston with a target pressure of 1.01325 bar (1 atm) is used. The Langevin piston temperature is set at 310 K throughout the simulation. The stability of the protein structure without load applied is verified from hydrogen bond dynamics as well as RMSD data obtained from the molecular dynamics trajectory.

Steered Molecular Dynamics Simulations

We use the steered molecular dynamics (SMD) approach[16] with a constant compression velocity as the protocol for simulating the force-induced deformation of the protein. SMD simulations mimic atomic force microscopy (AFM) studies of biomolecules, where the specimen is attached to a surface at one end and deformed at the other end by a cantilever moving with constant velocity. In SMD, the cantilever is replaced by a harmonic spring that is assigned to atoms that will be subject to displacement, and fixed boundary conditions are applied to the atoms that are selected to be restrained. The center of mass of the pulled atoms is constrained with a harmonic spring of stiffness k to move with velocity v in a specified direction $\vec{n}$. This approach applies the following additional energy potential to the system:

$$U(\vec{r}_1,\vec{r}_2,\ldots,t) = \frac{1}{2}k\left[vt - (\vec{R}(t) - \vec{R}_0)\cdot\vec{n}\right]^2 \qquad (1)$$

where t is the elapsed time in the simulation, $\vec{R}(t)$ is the current center of mass of the SMD atoms and $R_0(t)$ is the initial center of mass.

In our simulations, we select an SMD spring constant as $k = 1$ kcal/mol/Å^2 and a varying SMD displacement rate of $\dot{x} = 0.1$–25 m/s. Compared with other SMD studies,[36] the lowest effective loading rates used here (kv) are 10–100 times slower, reaching simulation times exceeding 20 ns. For the system size (approximately 40,000 atoms) and time-scales of interest, these simulations require parallel computing resources. The simulations are carried out on a Linux cluster at the Laboratory for Atomistic and Molecular Mechanics, as well on the BlueGene supercomputer at the San Diego Supercomputing Center.

The boundary conditions for our compression simulations consist of fixing the first two convolutions of

the protein structure at one end, while applying the moving harmonic constraint to atoms in two convolutions on the other end of the molecule. This approach enables us to achieve uniform loading conditions throughout the cross section. The fixity and moving harmonic constraints are applied to C_α atoms of all three molecules of the triple-helix.

We carry out a different simulation protocol to estimate stiffness of the system at quasi-static loading. In this simulation method, here referred to as small-perturbation simulations (SPS), the deformation velocity is kept constant initially until a desired displacement level is reached. At this point, the SMD velocity (initially 0.1 m/s, the slowest accessible rate) is reduced to zero, and the rate-dependent effects on force disappear while the end-to-end length oscillates around a displaced equilibrium point. The system is then equilibrated and ratio of the long-time average of the change in end-to-end length to the net force acting on the system is taken as the representative stiffness of the system at quasi-equilibrium loading.

Post-Processing and Data Analysis

Molecular visualization of trajectories are performed using the VMD program,[15] with H-bond cutoff distance and angle of 4 Å and 40°, respectively. Post-processing is carried out using MATLAB, where we use averaging scripts for force–displacement plots and curve fitting tools for studying the rate-dependence behavior. The best fit for rate-dependent plots is selected based on goodness criteria of the fit (e.g., R^2 values, confidence bounds) from a wide range of mathematical functions.

RESULTS

We summarize results from full-atomistic simulations in explicit solvent on the cell-puncture needle of bacteriophage T4.[18] The topology of the cell-puncture device and the atomistic structure of the needle domain are shown in Fig. 1a. The $(gp5C)_3$ domain of the molecular assembly represents the triple-helix beta-solenoid topology that is used to puncture through the outer cell membrane as part of the infection process. Following puncture, the gp5 lysozyme domains shown in Fig. 1a enzymatically breakdown the cell wall, after which the puncture device needle structure disassembles and viral DNA is injected into the cell through a larger cylindrical protein nanotube in the tail sheath. The protein assembly consists of three intertwined

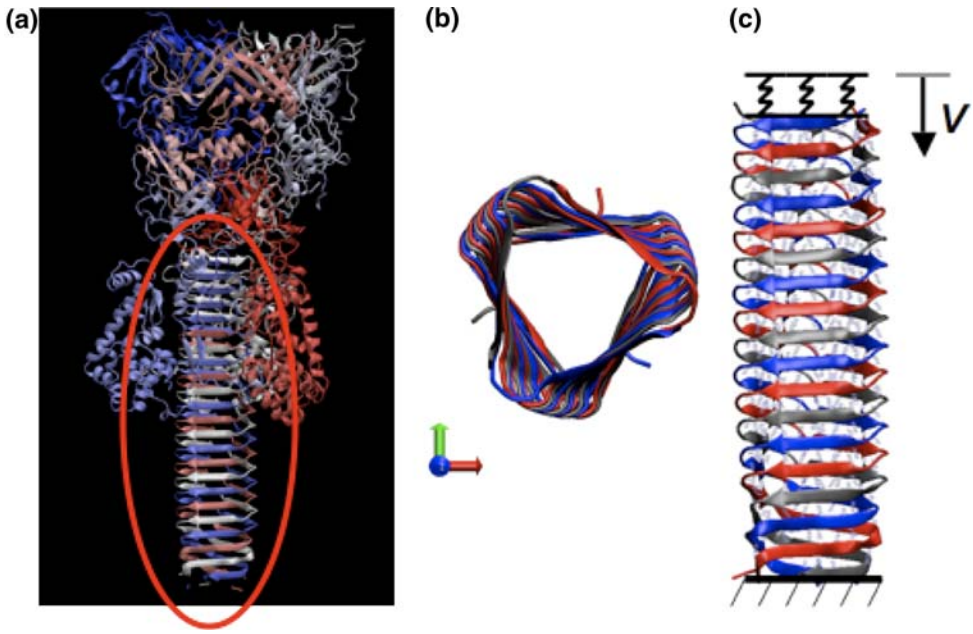

FIGURE 1. Schematics and simulation setup. Subplot (a) illustrates the molecular structure of the cell puncture device of bacteriophage T4 virus and the needle generally known as the gp5C domain encircled in red. The protein assembly consists of three polypeptide chains with identical folds that are symmetric rotations of each other around the helical axis. The triangular helical cross section rotates 3° with every convolution, as can be observed from the cross-section view shown in subplot (b). Atomistic simulations are performed to observe how the beta-helix topology of the needle behaves under compressive force, to clarify whether it could sustain large forces required to puncture through a cell membrane. Subplot (c) illustrates the setup for compression simulations, where the standard SMD protocol is implemented to apply compressive forces to the molecule with a constant loading rate.

polypeptide chains with identical folds that are symmetric rotations of each other around the helical axis. The triangular helical cross section consists of beta-sheets on each of the three sides with a slight twist of -3 degrees per strand, as can be observed from the cross-sectional view shown in Fig. 1b. Atomistic simulations are performed to observe how the beta-helix topology of the needle behaves under a compressive loading scenario similar to physiological conditions. The main goal of the simulations is to understand the mechanical properties of this specific topology and investigate whether it could sustain large forces required to puncture through a cell membrane. Figure 1c illustrates the setup for compression simulations, where the standard SMD protocol is implemented to apply compressive forces to the molecule at a constant loading rate.

We begin with systematically characterizing compressive strength of the structure at different loading rates. This is an important aspect as the simulations are carried out at much faster rates than experiments and extrapolation to slower rates is not straightforward. Figure 2a illustrates typical deformation profile of the triple-beta-helix under compression (results shown here from simulation with deformation speed $v = 25$ m/s). Significant "elastic" compression of the molecule can be observed before failure, in particular at the faster loading rates. As the structure is symmetric and an equilateral triangle at all cross-sections, there is no general weak axis based on the initial topology. This is because an equilateral triangle has the same moment of inertia along any axis passing through the center of mass, and hence the bending rigidity is uniform in all possible buckling directions. Moreover, further uniformity and interesting torsional properties are perhaps achieved through the true helical form of the molecular structure. We observe that failure occurs when the structure buckles with respect to a random "weakened" axis due to perturbations stemming from non-heterogeneous evolution of the topology under external force, H-bond rupture mediated by water molecules and thermal vibrations.

Force extension profiles for different loading rates are shown in Fig. 2b. The initial force extension behavior can be estimated by a linear elastic regime followed by nonlinear behavior toward failure, reminiscent of the buckling curves observed for most engineering materials. Rate-dependent elastic modulus of the system can be extracted from small deformation measurements where nonlinear instability effects are negligible, such that such that $E = kL/A$, where k is the initial stiffness, $L = 7.7$ nm is the length, and $A = 90$ Å^2 is the cross-sectional area of the molecule assuming a hollow section with 5 Å thickness representing the beta-sheet walls of the nanotube.

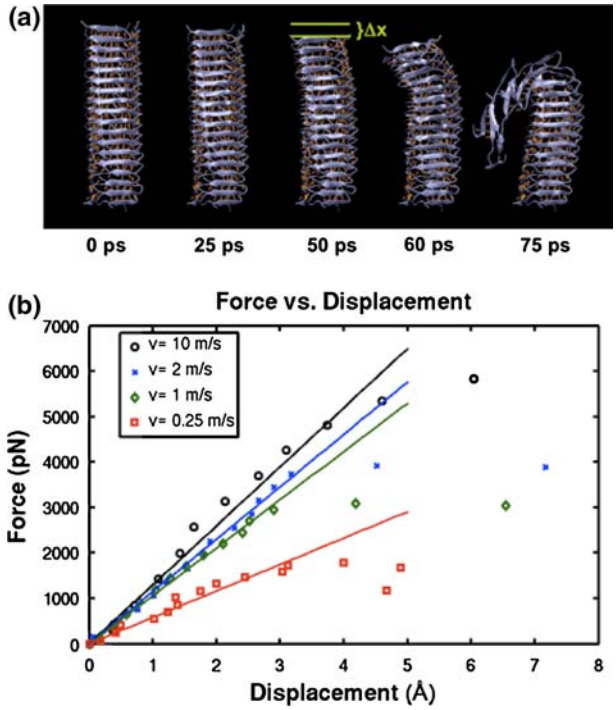

FIGURE 2. Snapshots of deformation, force extension plots. Subplot (a) illustrates typical deformation profile of the triple-beta-helix under compression (results from simulation with deformation speed $v = 25$ m/s). Significant compression of the molecule can be observed before failure, in particular at the faster loading rates. As the structure is symmetric and an equilateral triangle at all cross sections, there is no general weak axis based on the initial topology. Failure occurs when the structure buckles with respect to a random weak axis due to non-heterogeneous evolution of the topology under external force, H-bond rupture mediated by water molecules and thermal vibrations. Force extension profiles for different loading rates are shown in subplot (b). The initial force extension behavior can be estimated by a linear regime followed by nonlinear plastic-like behavior toward failure.

The peak force form each simulation can be plotted in force vs. log (v) space to illustrate rate-dependent mechanical behavior over roughly four orders of magnitude in time-scales. Figure 3a illustrates the rate-dependent failure force (approximated as the peak force from the simulation) of the triple-beta-helix as a function of the deformation speed. We observe that a power-law fit describes the behavior best, and can also be verified as the points lie on a straight line in a log-log curve. While most of the data lies in the nano-Newton force range, failure forces on the order of a few hundred picoNewtons are expected for this specific topology at slower, experimental deformation rates based on the power law description. Figure 3b illustrates dependence of the initial stiffness on the loading rate, where a different behavior from the power law is observed since the stiffness seems to converge to a finite value at increasingly fast pulling rates. Figure 3c shows that the peak force observed from simulations corresponds to the point at which the number of

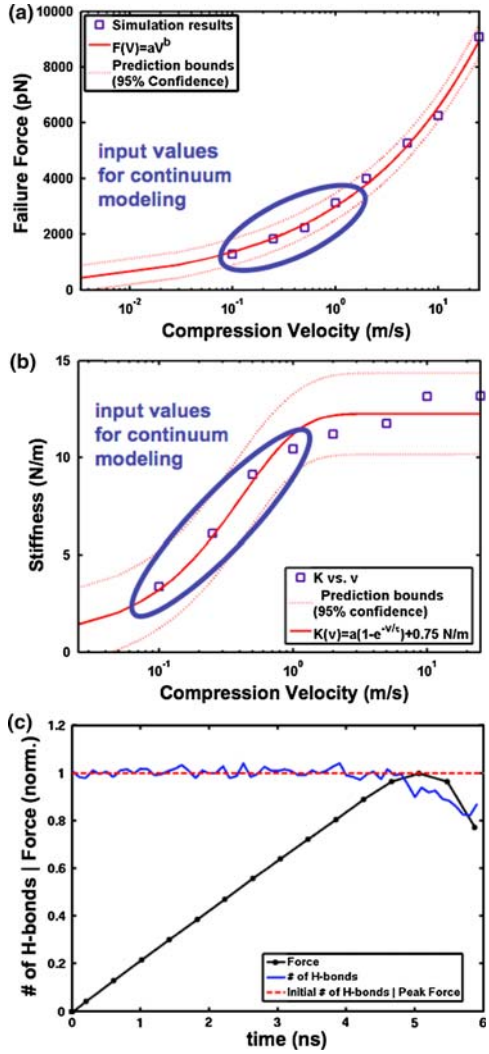

FIGURE 3. Rate dependence of force and stiffness. Subplot (a) illustrates the rate-dependent failure force of the cell-puncture needle as a function of the deformation speed. We observe that a power-law fit describes the behavior best, and can also be verified as the points lie on a straight line in a log–log curve. While most of the data lies in the nanoNewton force range, failure forces in the order of a few hundred picoNewtons are expected for this specific topology at slower, experimental deformation rates. Subplot (b) shows also rate-dependent behavior but is different from the power law behavior as the stiffness is observed to converge to a finite value at increasingly fast pulling rates. Based on our studies on small perturbation studies, we predict that a similar convergence is also likely in long time limit, slow deformation rates. Hence an exponential fit with a constant term makes most physical sense and also fits the data best. According to this, at faster rates, where the time-scale is too short for the system to respond to force (e.g., system is ''frozen'', or ''shocked''), the stiffness values around 12 N/m. At slower rates thermal vibrations and water-mediated H-bond rupture leads to softer response. In the long time limit, system will converge to its static loading stiffness, measured here to be approximately 0.75 N/m. An exponential function with constant term captures this rate-dependence effect well over all time-scales. Subplot (c) illustrates that the peak force corresponds a moment shortly after the decrease in the total number of H-bonds in the system, suggesting that H-bond rupture is a key event defining the onset of instability.

H-bonds in the system begins to decrease, leading to structural instability.

We predict that the stiffness of the molecule will converge to a finite value also at exceedingly slower rates, representing the quasi-static long time limit. Since time-scales of typical MD runs are much shorter than those in an ideal equilibrium-loading scenario, we carry out a different simulation protocol to estimate stiffness of the system at quasi-static rates. In these simulations (small-perturbation simulations, SPS), we study the thermal motion of the molecule around a displaced equilibrium point (see Methods section). Figures 4a and 4c show the loading scenario for the system as a function of time, while subplots (b) and (d) of Fig. 4 illustrate the change in end-to-end length of the system due to the external force for two different levels of strain. Our estimate for long-time limit yields 0.75 N/m for both cases, independent of the extent of deformation, supporting the result for the linear elastic fit for the initial deformation. We use this value as the constant term for the exponential fit to stiffness shown in Fig. 3b.

In the range of loading rates studied, we observe that the deformation profile of the system resembles those observed in typical buckling of columns, albeit the actual dynamics of the system appears to be much more complex. Mapping of the initial stiffness to the peak force is challenging without further validation from experiments. However, we attempt to provide a straightforward continuum type description of the rate-dependent failure load based on the initial stiffness value using Euler-Bernoulli beam buckling formulation. Since the exact boundary conditions of the system is unknown, we derive the parameter α that denotes end conditions of an idealized beam based on our values for force and stiffness for a small range of loading rates. The region of the fitting is denoted in Figs. 3a and 3b.

Figure 5a illustrates the simplified model of the structure for applying a continuum beam-buckling theory to the system, taking into account the rate-dependent initial stiffness of the system. The critical force that will lead to buckling can be estimated based on Euler theory[14] as:

$$P_{\mathrm{cr}} = \frac{\pi^2 EI}{(\alpha L)^2} \tag{2}$$

where the parameter α denotes the effective length scaling factor based on the boundary conditions of the buckling mode. The moment of inertia I, and cross-sectional area A are estimated from the atomistic model with a hollow cross-section assumption (for details, see also Keten and Buehler[20]). Figure 5b illustrates different constants that need to be used based on boundary conditions of the compressive

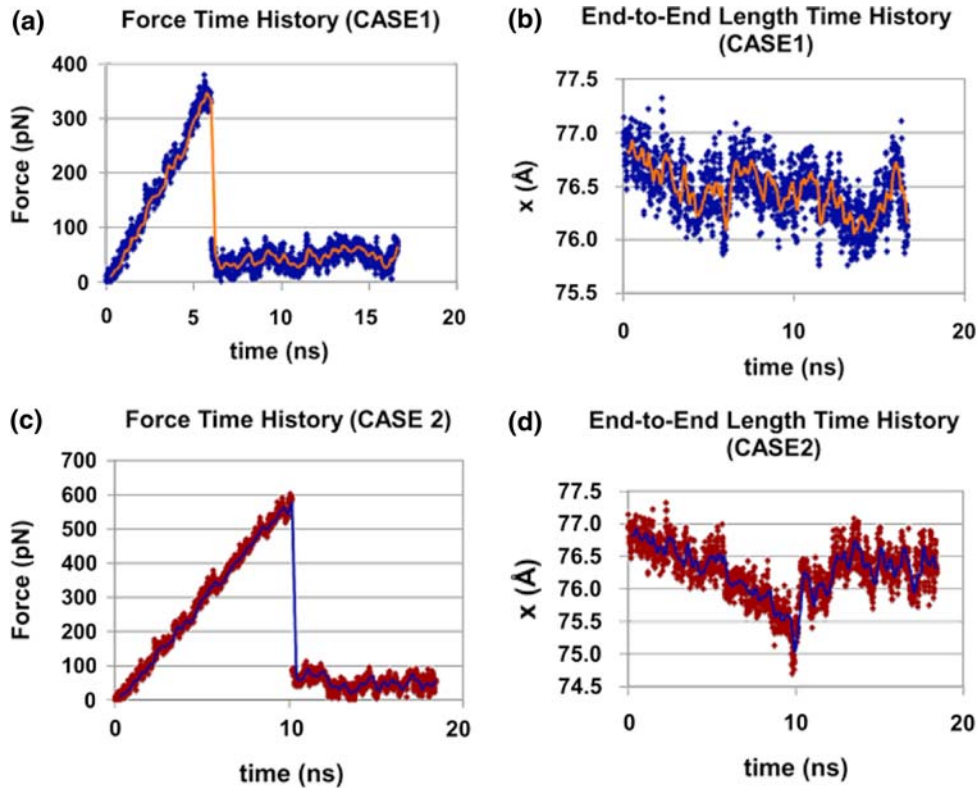

FIGURE 4. Small perturbation simulations (SPS). Subplots (a) and (c) show the loading scenario for the system as a function of time, while (b) and (d) illustrate the change in end-to-end length of the system due to the external force. In the SPS, deformation velocity is kept constant initially, until a desired displacement level is reached. At this point, the SMD velocity (initially 0.1 m/s, the slowest accessible rate) is reduced to zero, and the rate-dependent effects disappear. The system is then equilibrated for 8–10 ns and the averaged ratio of displacement to force is taken as the representative stiffness of the system at static loading. Our estimate for long-time limit turns out to be 0.75 N/m for both cases, independent of the extent of deformation, supporting the linear elastic fit for initial deformation.

loading. Since the exact boundary conditions of the system submerged in water is not precisely known in this case, we chose to select a value for the constant α that gives the best mapping between initial stiffness and failure force (taken here as the critical buckling load) prediction based on simulation results. The buckling formulation obtained can then be used to describe failure force at vanishing pulling rates based on the stiffness value obtained from small perturbation simulations. The selected region for stiffness and failure force values are shown in Figs. 3a and 3b where the dimensionless buckling parameter α is found to be 1.59 ± 0.14. The physical interpretation of this finding is that the boundary conditions adopted correspond to a case resembling fixed-free boundary conditions in typical Euler buckling with partial lateral restraints due to non-ideal loading conditions, fluid interaction or nonlinear material behavior.

Based on the constants obtained from the fitting to rate-dependent regime, one can also provide a prediction for quasi-static loading rates. Taking the stiffness result from SPS simulations where $k_{SPS} = 0.75$ N/m, we predict that the failure load at near static deformation rates will be roughly 225 pN; a value that could be tested experimentally. The power law fit error bounds shown in Fig. 3a agree well with this value. The fit can be modified to include this result as a constant term and matches well with the data from simulations, but more data points (in particular at experimental rates) is necessary before an accurate asymptotical value can be proposed.

DISCUSSION AND CONCLUSION

In this paper we have summarized results from atomistic simulations on the cell puncture device of bacteriophage T4 virus and have characterized, for the first time, the mechanical response of this biomolecular structure under external compression forces. Our simulation studies and the analysis of the underlying mechanisms have shed light on the underlying atomistic mechanisms. The simulations have provided important insight on the rate-dependent stability of this molecular assembly, illustrating that weak interactions such as H-bonds and electrostatic repulsion

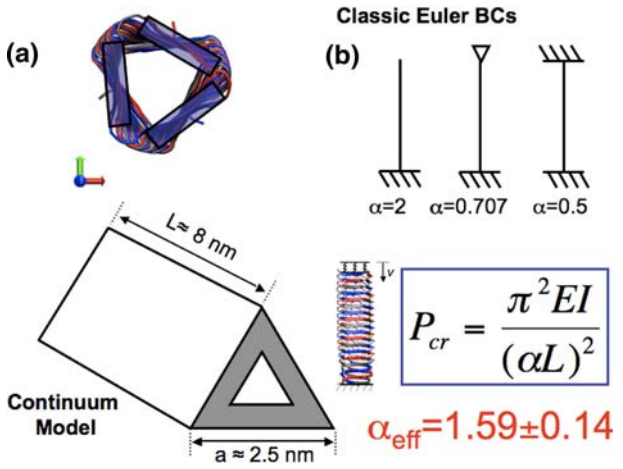

FIGURE 5. Schematics for continuum formulations. Subplot (a) illustrates the simplified model of the structure for applying a continuum buckling theory to the system, taking into account rate-dependent initial stiffness of the system. Subplot (b) illustrates different constants that need to be used based on boundary conditions of the compressive loading. Since the exact boundary conditions of the spring + beam system is unknown in our case, we can select a constant that gives the best mapping between initial stiffness and failure force. The buckling formulation obtained can then be used to describe failure force at vanishing pulling rates based on the stiffness value obtained from small perturbation simulations.

between charged side-chains govern the response to external force. This could be seen as similar to other biological materials such as cartilage where such weak interactions at the molecular scale also contribute significantly to the elastic modulus.[6]

Further, we have shown that an exponential fit with a constant term fits the rate-dependent stiffness data best, which makes physical sense as well since constant molecular stiffness values are expected at both extremely slow (quasi-static) and fast (shock) loading rates. Our analytical model enables us to predict the stiffness under a wide range of conditions and time-scales, including shock loading and quasi-static loading. A plausible explanation for this rate-dependence behavior is that at faster rates, where the time-scale is too short for the system to respond to force (e.g., system is "frozen", or "shocked"), the system has no time to readjust itself, water molecules have limited influence on H-bond dynamics, and thermal vibrations of the molecule are limited to very short timescales in which the dominant dynamic modes of the system can not be sampled adequately, hence the system reacts in a stiffer manner. At slower rates, thermal vibrations and water-mediated H-bond rupture leads to a softer response. In the long time limit, system will converge to its static loading stiffness, estimated here to be approximately 0.75 N/m, roughly fifteen times lower than the stiffness values observed under shock loading conditions. An exponential function with a constant term captures this rate-dependence effect well over all time-scales in an analytical model.

TABLE 1. Diameter (*D*) and persistence length (ξ_P) values for single biomolecules and biomolecular assemblies.

Biological molecule	Diameter *D* (nm)	Persistence length ξ_P (nm)	References
Polypeptide chain	0.5	0.4	[31,32]
Tropocollagen	2	11–16	[5,37]
Actin filament	6–8	3000–17000	[10,29]
Intermediate filament	10	1000–3000	[29]
Single beta-helix	3	900–1400	[20]
Triple beta-helix	3	800–14000	Present study[a]
Amyloid	9–11	10000–70000	[35]
Microtubule	25	1–8 10^6	[10]

[a]Present study, where we also include the persistence length calculations based on modulus values from faster loading rates.

The beta-helix topology exhibits extreme mechanical stability under compressive loads, reaching strength values close to nanoNewtons at fast deformation rates. The extreme rigidity of the molecule is most evident when it is compared with other biomolecular and inorganic nanostructures. Table 1 compares the diameter and persistence length of single biomolecules as well as biomolecular assemblies. Further experimental studies, both *in vivo* and *in vitro* are required to investigate how the specific topology of the cell-puncture device is suitable for its function and whether the molecular assembly can be optimized further by chemical and structural modifications, for example for the purpose of creating multifunctional, bioactive or mechanically rigid protein nanotubes.

The key contributions of this paper are:

- We have illustrated that stiffness and compressive strength of the molecule are strongly rate dependent (as it is the case of most biological matter). In particular at fast deformation rates this may be relevant in puncture impact on the surface of a cell. Our study indicates that the cell puncture device has a very high persistence length to diameter ratio, compared with other biomolecules, and can exhibit stiffness values much higher than that of a cell membrane (for instance, one study[9] shows $k_{CELL} \approx 0.27$ N/m for *E. coli*, much less than $k_{HELIX} = 0.75$–12 N/m as observed in this study).
- This is the first computational study at atomistic resolution that provides a detailed analysis of the compressive mechanical behavior of a single biological molecule, in this case a beta-solenoid type topology. The results and methods reported here can be readily applied to other protein structures, in particular to amyloids and prion proteins that show a similar molecular architecture.

The mechanical compliance of protein deposits with cells and surrounding tissue at oligomer and fibril length scales may have important implications for many pathological conditions such as neurodegenerative diseases.

- We have shown that the critical buckling load based on the Euler–Bernoulli beam theory could possibly be used to predict buckling phenomena at the nano-scale when coupled with atomistic information, in this case rate-dependent stiffness of the molecule. The agreement with failure force values obtained from molecular dynamics simulations supports this point. Investigation of the length-dependent stability of this particular topology either experimentally or by simulation is a necessity to determine whether or not Euler buckling is actually a valid model for this system.
- We have illustrated a basic structure–property–function relationship for this protein topology. The cell puncture needle is suitable for its function since: (1) The hollow triangular cross section is ideal for compressive loading as it has no particular weak axis and maximizes moment of inertia per unit area (compared with other cross-sections such as square or circle), increasing the failure force dramatically. (2) The structure utilizes weak H-bonds in compression to achieve significant compressive strength, an energetically efficient way of generating force to penetrate the cell membrane and a simpler method compared to more complex assembly mechanisms such as biomineralization. (3) The stiffness of the molecule is significantly higher than that of cells, for all deformation rates studied, making this system ideal for serving as a puncture needle. (4) The length of the molecule is long enough to span through the cell membrane but not significantly longer, allowing the molecule to have enough strength to serve its function without being susceptible to buckling at lower force levels.[20] Longer molecules would fall short of this capability, as the buckling force scales inversely with the square of the length according to Euler theory.

ACKNOWLEDGMENTS

This research was supported by the Office of Naval Research (Grant No.: N000140810844). The authors acknowledge a supercomputing grant at the San Diego Supercomputing Center (SDSC), as well as a large-scale computation grant from NSF TeraGrid system (Grant No.: MSS080030). The authors acknowledge helpful discussions with Prof. Matt Lang. J.F.R.A. acknowledges support from the Undergraduate Research Opportunities Program Office at MIT through the Paul E. Gray (1954) Endowed Fund for UROP.

REFERENCES

[1]Ackbarow, T., *et al.* Hierarchies, multiple energy barriers, and robustness govern the fracture mechanics of alpha-helical and beta-sheet protein domains. *Proc. Natl. Acad. Sci. USA* 104(42):16410–16415, 2007.
[2]Bernstein, F. C., *et al.* The Protein Data Bank: computer-based archival file for macromolecular structures. *J. Mol. Biol.* 112(3):535–542, 1977.
[3]Brändén, C.-I., and J. Tooze, Introduction to Protein Structure, 2nd ed. New York: Garland Publishing, xiv, 410 pp, 1999.
[4]Buehler, M. J. Nature designs tough collagen: explaining the nanostructure of collagen fibrils. *Proc. Natl Acad. Sci. USA* 103(33):12285–12290, 2006.
[5]Buehler, M., and S. Wong. Entropic elasticity controls nanomechanics of single tropocollagen molecules. *Biophys. J.* 93(1):37–43, 2007.
[6]Buschmann, M. D., and A. J. Grodzinsky. A molecular-model of proteoglycan-associated electrostatic forces in cartilage mechanics. *J. Biomech. Eng. Trans. ASME* 117(2): 179–192, 1995.
[7]Chiti, F., and C. M. Dobson. Protein misfolding, functional amyloid, and human disease. *Annu. Rev. Biochem.* 75:333–366, 2006.
[8]Cox, D. L., *et al.* The materials science of protein aggregation. *MRS Bull.* 30(6):452–457, 2005.
[9]da Silva, A., and O. Teschke. Dynamics of the antimicrobial peptide PGLa action on *Escherichia coli* monitored by atomic force microscopy. *World J. Microbiol. Biotechnol.* 21(6–7):1103–1110, 2005.
[10]Gittes, F., *et al.* Flexural rigidity of microtubules and actin-filaments measured from thermal fluctuations in shape. *J. Cell Biol.* 120(4):923–934, 1993.
[11]Govaerts, C., *et al.* Evidence for assembly of prions with left-handed beta 3-helices into trimers. *Proc. Natl Acad. Sci. USA* 101(22):8342–8347, 2004.
[12]Graether, S., *et al.* Beta-helix structure and ice-binding properties of a hyperactive antifreeze protein from an insect. *Nature* 406(6793):325–328, 2000.
[13]Hansma, H. G., *et al.* Probing biopolymers with the atomic force microscope: a review. *J. Biomater. Sci. Polym. Ed.* 11(7):675–683, 2000.
[14]Hibbeler, R. C. Statics and Mechanics of Materials. 2nd ed. Englewood Cliffs, NJ: Prentice Hall, p. 800, 2005.
[15]Humphrey, W., A. Dalke, and K. Schulten. VMD: visual molecular dynamics. *J. Mol. Graph.* 14(1):33–38, 1996.
[16]Isralewitz, B., M. Gao, and K. Schulten. Steered molecular dynamics and mechanical functions of proteins. *Curr. Opin. Struct. Biol.* 11(2):224–230, 2001.
[17]Kajava, A., J. Squire, and D. Parry. Beta-structures in fibrous proteins. *Adv. Protein Chem.* 73:1–15, 2006.
[18]Kanamaru, S., *et al.* Structure of the cell-puncturing device of bacteriophage T4. *Nature* 415(6871):553–557, 2002.
[19]Kellermayer, M. S. Z., *et al.* Reversible mechanical unzipping of amyloid beta-fibrils. *J. Biol. Chem.* 280(9):8464–8470, 2005.

[20]Keten, S., and M. J. Buehler. Large deformation and fracture mechanics of a beta-helical protein nanotube: atomistic and continuum modeling. *Comput. Methods Appl. Mech. Eng.* 197(41–42):3203–3214, 2008.
[21]Keten, S., and M. J. Buehler. Geometric confinement governs the rupture strength of H-bond assemblies at a critical length scale. *Nano Lett.* 8(2):743–748, 2008.
[22]Keten, S., and M. J. Buehler. Asymptotic strength limit of hydrogen bond assemblies in proteins at vanishing pulling rates. *Phys. Rev. Lett.* 100(19):198301, 2008.
[23]Kishimoto, A., *et al.* Beta-helix is a likely core structure of yeast prion Sup35 amyloid fibers. *Biochem. Biophys. Res. Commun.* 315(3):739–745, 2004.
[24]Knowles, T. P., *et al.* Role of intermolecular forces in defining material properties of protein nanofibrils. *Science* 318(5858):1900–1903, 2007.
[25]MacKerell, A. D., *et al.* All-atom empirical potential for molecular modeling and dynamics studies of proteins. *J. Phys. Chem. B* 102(18):3586–3616, 1998.
[26]Marszalek, P. E., *et al.* Mechanical unfolding intermediates in titin modules. *Nature* 402(6757):100–103, 1999.
[27]Mitraki, A., S. Miller, and M. J. van Raaij. Review: Conformation and folding of novel beta-structural elements in viral fiber proteins: the triple beta-spiral and triple beta-helix. *J. Struct. Biol.* 137(1–2):236–247, 2002.
[28]Mostaert, A. S., and S. P. Jarvis. Beneficial characteristics of mechanically functional amyloid fibrils evolutionarily preserved in natural adhesives. *Nanotechnology* 18(4): 044010, 2007.
[29]Mucke, N., *et al.* Assessing the flexibility of intermediate filaments by atomic force microscopy. *J. Mol. Biol.* 335(5):1241–1250, 2004.
[30]Nelson, M. T., *et al.* NAMD: a parallel, object oriented molecular dynamics program. *Int. J. Supercomput. Appl. High Perform. Comput.* 10(4):251–268, 1996.
[31]Oroudjev, E., *et al.* Segmented nanofibers of spider dragline silk: atomic force microscopy and single-molecule force spectroscopy. *Proc. Natl. Acad. Sci. USA* 99(Suppl 2): 6460–6465, 2002.
[32]Rief, M., *et al.* Reversible unfolding of individual titin immunoglobulin domains by AFM. *Science* 276(5315): 1109–1112, 1997.
[33]Rief, M., *et al.* The mechanical stability of immunoglobulin and fibronectin III domains in the muscle protein titin measured by atomic force microscopy. *Biophys. J.* 75(6): 3008–3014, 1998.
[34]Ritter, C., *et al.* Correlation of structural elements and infectivity of the HET-s prion. *Nature* 435(7043):844–848, 2005.
[35]Smith, J. F., *et al.* Characterization of the nanoscale properties of individual amyloid fibrils. *Proc. Natl Acad. Sci. USA* 103(43):15806–15811, 2006.
[36]Sotomayor, M., and K. Schulten. Single-molecule experiments in vitro and in silico. *Science* 316(5828):1144–1148, 2007.
[37]Sun, Y. L., *et al.* Direct quantification of the flexibility of type I collagen monomer. *Biochem. Biophys. Res. Commun.* 295(2):382–386, 2002.
[38]Wasmer, C., *et al.* Amyloid fibrils of the HET-s(218–289) prion form a beta solenoid with a triangular hydrophobic core. *Science* 319(5869):1523–1526, 2008.
[39]Yoder, M. D., S. E. Lietzke, and F. Jurnak. Unusual structural features in the parallel beta-helix in pectate lyases. *Structure* 1(4):241–251, 1993.